Orbital hybridization and magnetic coupling at cuprate-manganite interfaces driven by manganite doping

*Christoph Schlueter, Nan Yang, Claudio Mazzoli, Claudia Cantoni, Antonello Tebano, Daniele Di Castro, Giuseppe Balestrino, Pasquale Orgiani, Alice Galdi, Javier Herrero-Martín, Pierluigi Gargiani, Manuel Valvidares, and Carmela Aruta**

C. Schlueter
Photon Science, Deutsches Elektronen-Synchrotron DESY, Hamburg, 22603, Germany

N. Yang
School of Physical Science and Technology, ShanghaiTech University, 201210 Shanghai, China

C. Mazzoli
National Synchrotron Light Source III, Brookhaven National Laboratory, New York 11973, USA

C. Cantoni
Materials Science and Technology Division, Oak Ridge National Laboratory, Oak Ridge, 37831 TN, USA

A. Tebano, D. Di Castro, G. Balestrino
Department DICII, University of Roma Tor Vergata, I-00133 Rome, Italy and CNR-SPIN c/o University of Roma Tor Vergata, I-00133 Rome, Italy

P. Orgiani
CNR-SPIN Salerno, University of Salerno, I-84084 Fisciano, Italy and CNR-IOM, TASC National Laboratory, I-34149 Trieste, Italy

A. Galdi
CLASSE, Cornell University, Ithaca NY 14853, USA

J. Herrero-Martín, P. Gargiani, M. Valvidares
ALBA Synchrotron Light Source, Cerdanyola del Vallès, 08290 Barcelona, Spain

C. Aruta
CNR-SPIN c/o University of Roma Tor Vergata, I-00133 Rome, Italy

E-mail: carmela.aruta@spin.cnr.it

Keywords: superlattices, manganites, cuprates, interface reconstructions, magnetic interactions

Fundamental understanding of interface mechanisms that generate unexpected physical properties in the cuprate/manganite heterostructures is essential for possible applications as spintronic devices. Here $CaCuO_2/La_{1-x}Sr_xMnO_3$ (CCO/LSMO) superlattices are investigated, where the infinite-layer cuprate CCO does not have apical oxygen for Cu in the Ca-plane, so that the Mn–O–Cu

superexchange coupling can be only present at the MnO_2–(La,Sr)O–CuO_2 interface. Two different doping states for the manganites are studied, namely x = 0.1 and x = 0.3, corresponding to the ferromagnetic insulating and ferromagnetic metallic states, respectively, in the manganite phase diagram. Linear and circular dichroism in X-ray absorption by synchrotron radiation at Cu and Mn L-edges clearly demonstrate that in absence of apical oxygen in the cuprate block, the magnetic coupling between the LSMO and CCO is weakly ferromagnetic when LSMO is metallic, while it is antiferromagnetic when LSMO is insulating, along with an increased Cu $3d(3z^2\text{-}r^2)$ and Mn $3d(3z^2\text{-}r^2)$ orbital occupation. It is proposed that the Mn 3*d* valence band upward shift driven by the enhancement of Mn^{3+} content in the underdoped sample enhances the orbital hybridization. The stronger hybridization at the interface MnO_2–(La,Sr)O–CuO_2 gives rise to the antiferromagnetic coupling between cuprate and underdoped manganite.

1. Introduction

Cuprate/manganite interfaces have been investigated largely in the framework of heteroepitaxial structures of strongly electron correlated oxides, where the interactions at the interface between the constituent oxides results in a number of unexpected exotic properties.[1-4] In this context, controversial results on the magnetic coupling at cuprate/manganite interfaces are reported in the literature. In $YBa_2Cu_3O_7$/$La_{0.67}Ca_{0.33}MnO_3$ (YBCO/LCMO) multilayers an in-plane ferromagnetic (FM) component in the first interfacial Cu–O layer of YBCO is reported, which orders antiferromagnetically with the FM manganite layer.[5] X-ray spectroscopy studies suggest significant reconstruction of electronic orbitals at the interface. The resulting strong Mn–O–Cu covalent bond across the interface is responsible for the observed antiferromagnetic (AFM) coupling, giving rise to hole localization at the interface. The various competing parameters at the YBCO/LCMO interface were investigated by atomic-resolution electron-microscopy and spectroscopy.[6] The authors found an electron depletion-layer with a few nanometers thickness at interface due to the electron transfer from manganite to cuprate. However, they also reported electron enrichment in the manganite layer

very close to both interfaces YBCO/LSMO and LSMO/YBCO. Theoretical calculations describe the experimentally observed electron profile as a result of hybridization between the e_g orbitals of YBCO and LCMO in conjunction with a Cu/Mn atomic substitution in the LCMO layer. It has more recently been reported that the FM order of Cu moments in YBCO/LCMO is exclusively an "interface" effect due to orbital reconstruction, without contribution from the "bulk" CuO_2 planes.[7,8] In the same work, the fundamental role of covalency of the $3d(3z^2\text{-}r^2)$ orbitals for AFM coupling between the manganite and cuprate layer was reported, in accordance with previous studies.[5,6] The effect of the overlap of Cu and Mn 3*d* bands, close to the Fermi level, on the magnetic coupling was not considered, although the relevance of the Cu 3*d* bands in the magnetic exchange coupling with other magnetic systems has been demonstrated.[9] In this context, we investigate the cuprate/manganite interface in superlattices (SLs) with a structurally simple cuprate: the infinite layer (IL) compound $CaCuO_2$ (CCO). It consists exclusively of CuO_2 planes separated by bare Ca atoms, i.e., without oxygen apical to Cu. However, strongly oxidizing conditions, suppression of the electrostatic built-in potential and orbital reconstruction, could nevertheless cause apical oxygen at the interfaces of CCO based SLs as excess oxygen in the interface Ca plane. Apical oxygen located at the interface may drive charge transfer, offering an explanation for the interfacial $3d(3z^2\text{-}r^2)$ orbital occupation observed at several types of interfaces with CCO, as at the CCO/$La_{1-x}Sr_xMnO_3$ interface and in the superconducting CCO/$BaCuO_2$ or CCO/$SrTiO_3$ SLs.[10-13] Therefore, in this work, we use sufficiently oxidizing conditions for growth of well-oxygenated manganite blocks, but not strong enough to introduce excess oxygen at the CuO_2–Ca–MnO_2 interface. Furthermore, we use CCO blocks with thickness > 2 unit cells (uc) to prevent the formation of apical oxygen in chain-type structures.[14,15] The relevant role of the CuO chains in the interface magnetic coupling was previously reported in literature.[16] Thus, we here rule out any apical oxygen driven interplanar effect at the CuO_2–Ca–MnO_2 interface and focus our study exclusively on the possible effects of the hybridization between Cu and Mn mediated by oxygen at the MnO_2–(La,Sr)O–CuO_2 interface. The SL structures we study in this work consist of CCO blocks faced to the manganite $La_{1-x}Sr_xMnO_3$ (LSMO) with x = 0.3 (optimally doped, ferromagnetic metallic)

and with x = 0.1 (underdoped, ferromagnetic insulating). It has been recently reported that the ferromagnetic insulating manganite can be engineered at the interface to give rise to novel functionalities.[17] We will see that in our case, the insulating state of the LSMO affects the orbital hybridization and, thus, the magnetic coupling at the interface with CCO. We previously showed by hard X-ray photoelectron spectroscopy (HAXPES) that metallicity drives the overlap between Cu 3*d* and O 2*p* orbitals at the interfaces of CCO/LSMO SLs.[18] Therefore, while the effect of the orbital hybridization on the metallic and magnetic state of the perovkite based SLs has been largely reported in literature, we now take a different approach, looking at the interface orbital hybridization when changing the metallic state of the manganite. Linear dichroism (XLD) and circular dichroism (XMCD) in X-ray absorption measurements (XAS) allowed us to shed light on the still unexplored effect of LSMO metallicity on the magnetic coupling between the LSMO and CCO. By using optimally doped and underdoped manganite blocks in the SLs we modify the interface band overlap and thus orbital hybridization. This in turn modifies the exchange interaction which determines the magnetic coupling at the interface. We demonstrate that, in absence of apical oxygen in the cuprate block, the magnetic coupling between the LSMO and CCO is weakly ferromagnetic (FM) when LSMO is metallic, while it is antiferromagnetic (AFM) when LSMO is insulating. This is related to the Mn 3*d* electron occupation. Therefore, metallicity of the constituent blocks is a relevant parameter that has to be considered when dealing with interface interactions between cuprates and manganites.

2. Results and Discussion

CCO/LSMO SLs with different thickness of the constituent blocks and with different LSMO doping were grown by Pulsed Laser Deposition (PLD) on (110)$NdGaO_3$ (NGO) substrates. **Figure 1** (a) shows the transport properties of SLs with 3 uc of CCO and 14 uc of LSMO (3×14), having x = 0.3 (conducting) and x = 0.1 (insulating), hereafter called 3×14 SL03 and 3×14 SL01, respectively. The characteristic shape obtained for 3×14 SL03 indicates that the growth process results in well oxygenated manganite blocks and that interfacial effects are not strongly modifying the LSMO bulk

character. Non inverted annular bright field (ABF) transmission electron microscope (STEM) image of the 3×14 SL03 shown in Figure 1(b) demonstrates the absence of oxygen atoms in the Ca-planes (i.e. dark contrast spot within the light blue box).[19] The CCO block can be therefore considered in the IL state. Apical oxygen acting as a bridge between the two different constituent blocks is only present at the MnO_2–(La,Sr)O–CuO_2 and not at the CuO_2–Ca–MnO_2 interface. STEM image also shows that interfaces are abrupt with some interdiffusion of about 1 uc and confirms the expected thickness of the $CaCuO_2$ block , i.e. 3 uc. Structural characterizations by x-ray reflectivity and x-ray diffraction measurements reported in Supporting Information also demonstrate the good quality of the SL structures. Further structural characterization on the same or similar samples were previously reported.[10,18]

The XMCD at the Mn and Cu $L_{2,3}$-edges of 3×14 SL03 are shown in **Figure 2** (a) and (b), respectively. The XMCD at the Cu $L_{2,3}$-edge is very weak and the signal was detectable in normal incidence (NI) and at 6 T applied magnetic field only. Comparison between XMCD spectra of the Mn and the Cu $L_{2,3}$-edges shows FM coupling (despite the signal being quite weak) between the LSMO and CCO block in case of 3×14 SL03. The XMCD results of a SL with 3 uc of CCO and 4 uc of LSMO having x=0.3 (called 3×4 SL03) are shown in Figure 2(c) and (d). When decreasing the thickness of the LSMO block to 4 uc, the XMCD signal at Cu L-edge of 3×4 SL03 reported Figure 2(d) becomes lower than in the case of 3×14 SL03 reported in Figure 2(b), even though it was better detectable because the CCO block was less buried. We can observed that the FM coupling occurs also in grazing incidence (GI) and at lower magnetic field, i.e., 1 T. The XMCD signals at the Mn and Cu $L_{2,3}$ edges both decrease with decreasing the thickness of the LSMO block from 14 uc to 4 uc. This finding demonstrates that the magnetization of CCO is depending on the thickness or some induced intrinsic property of the LSMO. However, the decreasing of the XMCD signal at the Cu $L_{2,3}$ edge does not decrease by the same amount as the XMCD signal at the Mn $L_{2,3}$ edge. This makes us think the magnetization in CCO is not induced by the whole LSMO block, but it is mainly related to the interface layers of LSMO. It is worth noting that the XMCD shape of 3X4 SL03 is different from

that one of 3X14 SL03. This can be related to the increased Mn^{4+} content at the interface, in agreement with the high energy shift of XAS spectra as reported in Supporting Information.[10,20,21]

To understand the origin of the different XMCD in CCO, we measured the 3×14 SL01, where the manganite block is underdoped and, thus, in the FM insulating state. Interestingly, the comparison of the XMCD spectra at the Mn and the Cu $L_{2,3}$-edges of **Figure 3** (a) and (b) reveals an opposite relative orientation of the Mn and Cu magnetic moments with respect to the case of LSMO with x = 0.3 manganite block (Figure 2). Therefore, the magnetic coupling becomes AFM when the CCO block is faced to an underdoped manganite. However, the XMCD signal at the Cu $L_{2,3}$ edge of 3×14 SL01 (Figure 3(b)) is also larger than in the case of 3×14 SL03 (Figure 2(b)).

Following previous findings by HAXPES, in insulating SLs the Mn 3*d* valence band shifts upward, increasing the energy overlap of the interfacial O 2*p* of the LSMO block and Cu 3*d* orbitals.[18] In the conducting SLs the Mn 3*d* valence band shifts downward, decreasing the energy overlap of the interfacial O 2*p* and Cu 3*d* orbitals. Therefore, we expect that in SLs with insulating manganite, the stronger hybridization at the interface MnO_2–(La,Sr)O–CuO_2 gives rise to the AFM coupling between cuprate and manganite.[3,6,7]

To corroborate our hypothesis we report XLD results, providing information on the orbital anisotropy. XAS measurements and XLD calculation at Cu L_3-edge are shown in **Figure 4** (a) for 3×14 SL03 and 3×14 SL01. Since XAS is probing holes mostly in $3d(x^2\text{-}y^2)$ and $(3z^2\text{-}r^2)$ e_g states in vertical (V) and horizontal (H) polarizations respectively, the positive XLD spectra, obtained as a difference V-H, demonstrate that the single hole ($3d^9$ single electron) is prevalently in the $3d(x^2\text{-}y^2)$ orbital, which is the higher energy level, in both the 3×14 SL03 and SL01. XAS spectra at Cu L_3-edge of both 3×14 SL03 and SL01 samples show an evident asymmetry of the peak shape because of the contribution of the interface component at lower photon energy.[7] Indeed, this interface component decreases with increasing the CCO thickness (see **Figure 5**). The XLD of bottom panel of Figure 4(a) shows a shift to lower photon energy in SL01 with respect to SL03. This can be the signature of the increased delocalization of the holes, which we propose as the result of the higher hybridization of CCO and

LSMO bands. Furthermore, the shift to lower photon energy is mainly due to the interface component, as highlighted in Supporting Information, demonstrating that the higher hybridization plays a major role at the interface between CCO and LSMO.

XAS measurements and XLD calculation at the Mn $L_{2,3}$-edge are reported in Figure 4(b) for SLs with the same stacking sequence but LSMO blocks having different doping, i.e. x = 0.3 and x=0.1. The XLD shape of bottom panel of Figure 4(b) shows that e_g electrons of Mn^{3+} ions preferentially occupy $3d(3z^2\text{-}r^2)$ orbitals, which are at lower energy than the prevalently empty $3d(x^2\text{-}y^2)$ orbitals, in both the 3×14 SL03 and SL01.[22,23] XLD also shows that the Mn $3d(3z^2\text{-}r^2)$ occupation in SL01 is higher than in SL03. The valence state of Mn ion is nominally 3.1 when x = 0.1 and 3.3 when x = 0.3, therefore we expect more Mn^{4+} ($3d^3$) and less Mn^{3+} ($3d^4$) in the SL03 with respect to the SL01 samples. This is confirmed by the XAS spectra energy shift to higher photon energy of 3×14 SL03 with respect to 3×14 SL01, as reported in Supporting Information. Since Mn^{4+}, unlike the case of Mn^{3+}, cannot distort its octahedral environment by Jahn-Teller effect, the enhancement of XLD intensity in the 3×14 SL01 is in agreement with the increase of Mn^{3+} content.[24] In addition, the metallic state is orbitally disordered.[25] The increased Mn^{3+} content in the insulating orbitally ordered state can induce a higher Cu 3*d* – O 2*p* – Mn 3*d* band overlap in the SL01 sample mediated by the out-of-plane $3d(3z^2\text{-}r^2)$ orbitals of both Cu 3*d* and Mn 3*d*.

It has been reported that decreasing the LSMO layer thickness the preferential occupation of the Mn $3d(3z^2\text{-}r^2)$ and Cu $3d(3z^2\text{-}r^2)$ orbitals increases.[10,18] The interface orbital occupation of the CCO block is now better emphasized by measuring samples with different CCO thickness. We fixed LSMO at 4 uc and changed the CCO thickness from 3 uc to 6 uc and 9 uc (3×4 SL03, 6×4 SL03 and 9×4 SL03). We keep the thickness of the CCO block very thin (3-9 uc) to explore mainly interface effects. XAS results at the Cu L_3 edge are reported in Figure 5 (a), where the E//ab configuration corresponds to the XAS measured in V polarization and the E//c configuration is isolated by combining the V and H polarization spectra.[26] Two components can be noticed in the fit of the E//ab configuration and only one component in the E//c configuration. This last component at lower energy is the contribution

from the Cu^{2+} ions close to the interface.[7] The behavior of the relative weight of such interface component with different CCO uc in Figure 5(b) shows the expected larger contribution in the sample with the thinnest CCO block (3×4 SL03), as well as the anisotropy behavior demonstrates that the interface component is more isotropic in SLs with thinner CCO blocks. However in all cases the interface component shows Cu $3d(3z^2\text{-}r^2)$ preferential orbital occupation. Furthermore, hole or electron doping would be evidenced by additional peaks centered at 1.5 eV and 2.6 eV above the Cu^{2+} peak, respectively; from the residual of the fit, no significant spectral weight is detected at those energies, indicating that the doping of the CCO layer is negligible.[26] A similar fitting procedure of XAS spectra at the Cu L_3 edge was applied for the 3X14 SL03 and 3X14 SL01, as reported in Supporting Information. Remarkably, the results indicate that the relative weight of the interface component does not significantly change with doping, but the anisotropy does being larger for the undoped sample.

The magnetic anisotropy of 3X14 SL03 and 3X14 SL01 was investigated by X-ray magnetic linear dichroism (XMLD) at the Mn $L_{2,3}$-edge spectra, as reported in **Figure 6** (a). It can be observed that XMLD spectra all have the same qualitative behavior. The similar shape in 0 T and 6 T is a clear indication that the AFM and FM spin systems have the same orientation, because of the directional coupling by exchange bias between the spins in the AFM regions and those in the adjacent FM regions.[27] The line shapes are similar to those previously reported for thin LSMO films with AFM and FM magnetization easy axes oriented along the c-axis.[28,29] In the case of 3×14 SL01 the signal is more dichroic than the 3×14 SL03, as an indication of a stronger magnetic anisotropy, which follows the Mn $3d(3z^2\text{-}r^2)$ orbital occupation. The AFM and FM phases of both the 3×14 SL03 and SL01 sample can coexist on the nanometer scale at the interface.[20] Indeed, the XMCD at Mn $L_{2,3}$-edge of 3×4 SL03 with the thinnest LSMO blocks decreases, demonstrating that the FM is suppressed in the thin LSMO layers due to the interface AFM domains.

3. Conclusion

We observe different magnetic coupling between the cuprate and manganite blocks in CCO/LSMO SLs depending on the metallicity of the LSMO units. The magnetic coupling is of FM type, when the manganite is optimally doped, namely FM-metallic (3×14 SL03) while it becomes AFM type, when the manganite is underdoped, namely FM-insulating (3×14 SL01). Since no relevant amount of apical oxygen atoms in the Ca plane at the CuO_2–Ca–MnO_2 interface was detected by STEM, we can rule out superexchange interaction mediated by the O 2*p* orbitals at that interface. On the contrary, at the MnO_2–(La,Sr)O–CuO_2 interface, the O 2*p* orbitals in the (La,Sr)O plane may allow FM superexchange interaction between the Cu $3d(3z^2\text{-}r^2)$ and the empty Mn $3d(3z^2\text{-}r^2)$ orbitals in SL03. When the manganite is insulating (e.g. SL01) the higher overlap of Cu 3*d* and Mn 3*d* bands facilitates exchange interaction and we observe AFM coupling between Cu $3d(3z^2\text{-}r^2)$ and Mn $3d(3z^2\text{-}r^2)$ orbitals. Therefore, the coupling to the *d* bands near the Fermi level is driven by the Mn^{3+} electron occupation in the insulating state. This induces the higher hybridization between Cu and Mn orbitals close to the interface which, in turn, strongly influences the spin polarization and the Cu 3*d* spin moment at the interface. Our results demonstrate that changing the manganite doping is an effective method to control the magnetic coupling at the cuprate/manganite interface and, in a broader context, to manipulate the functional properties in oxide-based heterostructures.

4. Experimental Section

Superlattices deposition: Samples were grown in University of Rome Tor Vergata (Rome, Italy) by PLD on (110)$NdGaO_3$ (NGO) substrates. NGO has a pseudocubic in-plane lattice parameter a = 3.87 Å, giving a very low lattice mismatch with the CCO and the pseudocubic LSMO in plane lattice parameters of 3.84Å and 3.87Å, respectively. NGO also demonstrated to be the most suitable substrate to grow the CCO samples, acting as a template for the peseudomorphic stabilization of the infinite layer phase.[30]

The oxygen partial-pressure was optimized to obtain the best metal-insulator transition temperature in our LSMO bare films, but avoiding excess oxygen at the interface of the SLs. The investigated samples were grown in 8×10^{-1} mbar of O_2 followed by quenching to room temperature in 1 bar of O_2. CCO/LSMO SLs with different number of CCO and LSMO layers were grown for the study. We have grown SLs with 3 uc of CCO and 14 uc of LSMO with x = 0.3 and x = 0.1. In the case of SLs with LSMO having x = 0.3 we fixed at 4 uc the LSMO and changed the thickness of the CCO block:, namely, 3 uc, 6 uc and 9 uc of CCO. The number of *N* repetition of the CCO/LSMO bilayers, are *N*=20 for the 3×4 and 6×4 SLs, and *N*=18 for the 9×4 and 3×14 SLs.

Transport measurements: Electrical transport measurements were carried out by the standard four-probe dc technique. Silver epoxy electrical contacts were provided before the film deposition directly on the substrate in Van der Pauw configuration with a pulsed bias and reversed current.[31] For the resistivity calculation, the thickness value was obtained by x-ray reflectivity and x-ray diffraction measurements.

Transmission Electron Microscopy: Microscopy measurements were performed with a 200 kV electron microscope (JEM-ARM200F) equipped with annular bright field (ABF) and dark field (ADF) detectors as well as a spherical aberration correction system for STEM.[32] In particular, the ABF imaging enables us to directly see light atoms, such as oxygen. Different samples and imaging regions were measured proving comparable results on the interface and structural properties, also in agreement with previous measurements on similar samples.[10,12]

X-ray Absorption Dichroim: X-ray absorption linear and magnetic dichroism (XLD and XMCD) experiments at the Cu and Mn $L_{2,3}$ edges were performed at the BL29 BOREAS beamline at the ALBA synchrotron radiation facility (Barcelona, Spain).[33] Total electron yield detection mode was used, which has a probing depth of about 10 nm. Consequently, several interfaces contributed to the measured signal. A magnetic field up to 6 Tesla was applied in the direction of the photon beam using the high-field vector magnet (HECTOR) end station of BOREAS beamline. The temperature was changed from room temperature down to 30 K.

The sample surface (*ab*-plane) was oriented vertically in the laboratory reference system and illuminated by the incident beam radiation in normal incidence (NI), i.e. parallel to the crystal c-axis, and in grazing incidence (GI) with the direction forming a 60 degrees angle with the surface normal. As usual, XLD measurements were obtained with linear vertical (V) and horizontal (H) polarized light, and XMCD with almost 100% right- and left-handed circular polarizations. In GI geometry with H-polarization the electric field vector *E* of the synchrotron radiation was at 30 degrees with respect to the c-axis. Consequently, 75% of the XAS intensity was obtained from the empty states with out-of-plane symmetry.

X-ray Magnetic Linear Dichroism: The difference between the XLD spectra taken below the magnetic transition temperature and at room temperature is called XMLD (X-ray magnetic linear dichroism).

The signal intensity of X-ray absorption can be written as:

$I \approx \cos^2(\boldsymbol{E}\cdot\boldsymbol{Q})\langle\boldsymbol{Q}\rangle + \cos^2(\boldsymbol{E}\cdot\boldsymbol{M})\langle\boldsymbol{M}^2\rangle_T$

where $\langle\boldsymbol{Q}\rangle$ is the quadrupole moment of the charge and $\langle\boldsymbol{M}^2\rangle_T$ the square magnetic moment. Therefore, both orbital and magnetic anisotropy can be probed by XLD, if the magnetic moment of the spin system has a component in the plane perpendicular to the propagation direction of the X-ray beam.[34-36] Magnetic anisotropy is only visible in the XLD spectra when the measurements are performed below the magnetic transition temperature. If we assume that the orbital anisotropy is negligibly sensitive to temperature changes, the difference between the XLD signals below the magnetic transition temperature (both orbital and magnetic anisotropy) and at room temperature (orbital anisotropy only) gives information on the anisotropy related to magnetization (both AFM and FM). However, measurements with 6 T applied magnetic field are primarily sensitive to the AFM anisotropy, if the applied magnetic field is able to saturate the FM phase in the direction of the beam in the given measurement geometry.

Fitting of the Cu L_3 XAS spectra: The fit of the Cu L_3 XAS spectra was performed with a superposition of Gaussian curves after subtracting a first order Shirley background.[26] In the energy range from 922

to 930 eV, the E//ab spectrum contains the contributions from both Cu^{2+} in the $3d(3z^2\text{-}r^2)$ orbital configuration (typical of cuprate superconductors and fully dichroic) and the interface component, while the E//c spectrum only contains the interface contribution.[7, 37] The E//ab data were hence fitted with two Gaussian curves; the energy position and width of the interface component were fixed to the values obtained by the fit of the single Gaussian peak in the E//c data, and only its intensity was allowed to vary.

Supporting Information
Supporting Information is available from the Wiley Online Library or from the authors.

References

[1] Yaohua Liu and Xianglin Ke, *J. Phys.: Condens. Matter* **2015**, *27*, 373003.

[2] A. Bhattacharya and S. J. May, *Annu. Rev. Mater. Res.* **2014**, *44*, 65–90.

[3] J. Chakhalian, J. W. Freeland, A. J. Millis, C. Panagopoulos and J. M. Rondinelli, *Rev. Mod. Phys.* **2014**, *86*, 1189.

[4] H. Y. Hwang, Y. Iwasa, M. Kawasaki, B. Keimer, N. Nagaosa, and Y. Tokura, *Nat. Mater.* **2012**, *11*, 103.

[5] J. Chakhalian, J. W. Freeland, H.-U. Habermeier, G. Cristiani, G. Khaliullin, M. van Veenendaal, B. Keimer, *Science* **2007**, *318*, 1114.

[6] J. Salafranca, J. Rincón, J. Tornos, C. León, J. Santamaria, E. Dagotto, S. J. Pennycook, and M. Varela, *Phys. Rev. Lett.* **2014**, *112*, 196802-196807.

[7] K. Sen, E. Perret, A. Alberca, M. A. Uribe-Laverde, I. Marozau, M. Yazdi-Rizi, B. P. P. Mallett, P. Marsik, C. Piamonteze, Y. Khaydukov, M. Döbeli, T. Keller, N. Biškup, M. Varela, J. Vašátko, D. Munzar, and C. Bernhard, *Phys. Rev. B* **2016**, *93*, 205131.

[8] M. A. Uribe-Laverde, S. Das, K. Sen, I. Marozau, E. Perret, A. Alberca, J. Heidler, C. Piamonteze, M. Merz, P. Nagel, S. Schuppler, D. Munzar, and C. Bernhard, *Phys. Rev. B* **2014**, *90*, 205135.

[9] M. G. Samant, J. Stöhr, S.S.P. Parkin, G. A. Held, B.D. Hermsmeier, and F. Herman, *Phys. Rev. Lett.* **1994**, *72*, 1112.

[10] N. Yang, D. Di Castro, C. Aruta, C. Mazzoli, M. Minola, N. B. Brookes, M. Moretti Sala, W. Prellier, O. I. Lebedev, A. Tebano,1 and G. Balestrino, *J. Appl. Phys.* **2012**, *112*, 123901.

[11] C. Aruta, G. Ghiringhelli, C. Dallera, F. Fracassi, P. G. Medaglia, A. Tebano, N. B. Brookes, L. Braicovich, and G. Balestrino, *Phys. Rev. B* **2008**, *78*, 205120.

[12] D. Di Castro, C. Cantoni, F. Ridolfi, C. Aruta, A. Tebano, N. Yang, and G. Balestrino, *Phys. Rev. Lett.* **2015**, *115*, 147001.

[13] C. Aruta, C. Schlueter, T.-L. Lee, D. Di Castro, D. Innocenti, A. Tebano, J. Zegenhagen, and G. Balestrino, *Phys. Rev. B* **2013**, *87*, 155145.

[14] Z. Zhong, G. Koster, and P. J. Kelly, *Phys. Rev. B* **2012**, *85*, 121411.

[15] D. Samal, Haiyan Tan, H. Molegraaf, B. Kuiper, W. Siemons, S. Bals, J. Verbeeck, G. Van Tendeloo, Y. Takamura, E. Arenholz, C. A. Jenkins, G. Rijnders, and G. Koster, *Phys. Rev. Lett.* **2013**, *111*, 096102.

[16] S. W. Huang, L. Andrew Wray, Horng-Tay Jeng, V. T. Tra, J. M. Lee, M. C. Langner, J. M. Chen, S. Roy, Y. H. Chu, R. W. Schoenlein, Y.-D. Chuang and J.-Y. Lin, *Sci. Rep.* **2015**, *5*,16690.

[17] Weiwei Li, B. Zhu, Qian He, A. Y. Borisevich, Chao Yun, Rui Wu, Ping Lu, Zhimin Qi, Qiang Wang, Aiping Chen, Haiyan Wang, S. A. Cavill, K. H. L. Zhang, and J. L. MacManus-Driscoll, *Adv. Sci.* **2019**, *7*, 1901606.

[18] C. Schlueter, C. Aruta, N. Yang, A. Tebano, D. Di Castro, G. Balestrino, and T. L. Lee, *Phys. Rev. Mater* **2019**, *3*, 094406.

[19] Yi Wang, U. Salzberger, W. Sigle, Y. E. Suyolcu, P. A. van Aken, *Ultramicroscopy*, **2016**, *168*, 46–52.

[20] A. Tebano, C. Aruta, P. G. Medaglia, F. Tozzi, and G. Balestrino, A. A. Sidorenko, G. Allodi, and R. De Renzi, G. Ghiringhelli, C. Dallera, and L. Braicovich, N. B. Brookes, *Phys. Rev. B* **2006**, *74*, 245116.

[21] M. Abbate, F. M. F. de Groot, J. C. Fuggle, A. Fujimori, O. Strebel, F. Lopez, M. Domke, G. Kaindl, G. A. Sawatzky, M. Takano, Y. Takeda, H. Eisaki, S. Uchida, *Phys. Rev. B* **1992**, *46*, 4511.

[22] C. Aruta, G. Ghiringhelli, A. Tebano, N. G. Boggio, N. B. Brookes, P. G. Medaglia, and G. Balestrino, *Phys. Rev. B* **2006**, *73*, 235121.

[23] D. Pesquera, G. Herranz, A. Barla, E. Pellegrin, F. Bondino, E. Magnano, F. Sánchez & J. Fontcuberta, *Nat. Commun*. **2012**, *3*, 1189.

[24] C. Aruta, G. Balestrino, A. Tebano, G. Ghiringhelli and N. B. Brookes, *Europhys. Lett.* **2007**, *80*, 37003.

[25] Y. Tokura and N. Nagaosa, *Science* **2000**, *288*, 462.

[26] A. Galdi, P. Orgiani, C. Sacco, B. Gobaut, P. Torelli, C. Aruta, N. B. Brookes, M. Minola, J. W. Harter, K. M. Shen, D. G. Schlom, and L. Maritato, *J. Appl. Phys.* **2018**, *123*, 123901, *and references 18-21 therein.*

[27] F. Nolting, A. Scholl, J. Stöhr, J. W. Seo, J. Fompeyrine, H. Siegwart, J.-P. Locquet, S. Anders, J. Lüning, E. E. Fullerton, M. F. Toney, M. R. Scheinfeink, and H. A. Padmore, *Nature* **2000**, *405*, 767.

[28] C. Aruta, G. Ghiringhelli, V. Bisogni, L. Braicovich, N. B. Brookes, A. Tebano, and G. Balestrino, *Phys. Rev. B* **2009**, *80*, 014431.

[29] S. J. Carreira, M. H. Aguirre, J. Briatico and L. B. Steren, *RSC Adv.* **2019**, 9, 38604-38611.

[30] G. Balestrino, R. Desfeux, S. Martellucci, A. Paoletti, G. Petrocelli, A. Tebano, B. Mercey, and M. Hervieu, *J. Mater. Chem*. **1995**, *5*, 1879.

[31] L. J. van der Pauw, *Philips Tech. Rev.* **1958**, *20*, 220.

[32] C. Cantoni, J. Gazquez, F. Miletto Granozio, M. P. Oxley, M. Varela, A. R. Lupini, S. J. Pennycook, C. Aruta, U. Scotti di Uccio, P. Perna, and D. Maccariello, *Adv. Mater.* **2012**, *24*, 3952–3957.

[33] A. Barla, J. Nicolás, D. Cocco, S. M. Valvidares, J. Herrero-Martín, P. Gargiani, J. Moldes, C. Ruget, E. Pellegrin, S. Ferrer, *J. Synchrotron Radiat.* **2016**, *23*, 1507.

[34] P. Kuiper, B. G. Searle, P. Rudolf, L. H. Tjeng, and C. T. Chen, *Phys. Rev. Lett.* **1993**, *70*, 1549.

[35] G. van der Laan, B. T. Thole, G. A. Sawatzky, J. B. Goedkoop, J. C. Fuggle, J. M. Esteva, R. Karnatak, J. P. Remeika, and H. A. Dabkowska, *Phys. Rev. B* **1986**, *34*, 6529.

[36] J. Stöhr and S. Anders, *IBM J. Res. Dev.* **2000**, *44*, 535.

[37] J. Fink, N. Nucker, E. Pellegrin, H. Romberg, and M. Knupfer, *J. Electron Spectrosc. Relat. Phenom.* **1994**, 66, 395.

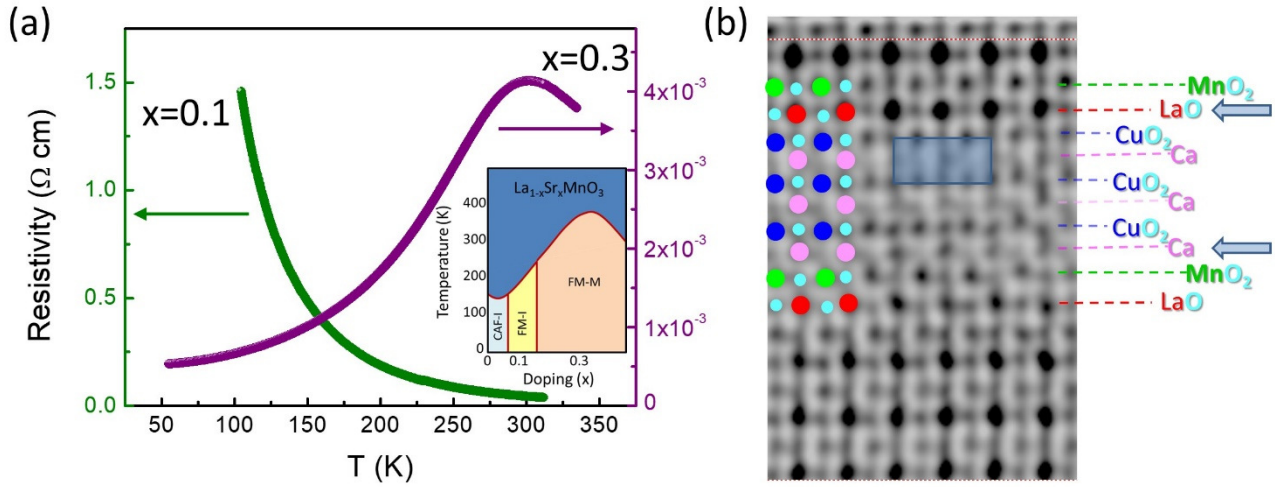

Figure 1. (a) Temperature dependence of the resistivity of SLs with x = 0.1 (3X14 SL01) and with x = 0.3 (3×14 SL03). A schematic phase diagram with different stoichiometry is shown in the inset. (b) Non-inverted ABF STEM image of the 3×14 SL03 sample. The arrows indicate the MnO_2–(La,Sr)O–CuO_2 and CuO_2–Ca–MnO_2 interfaces.

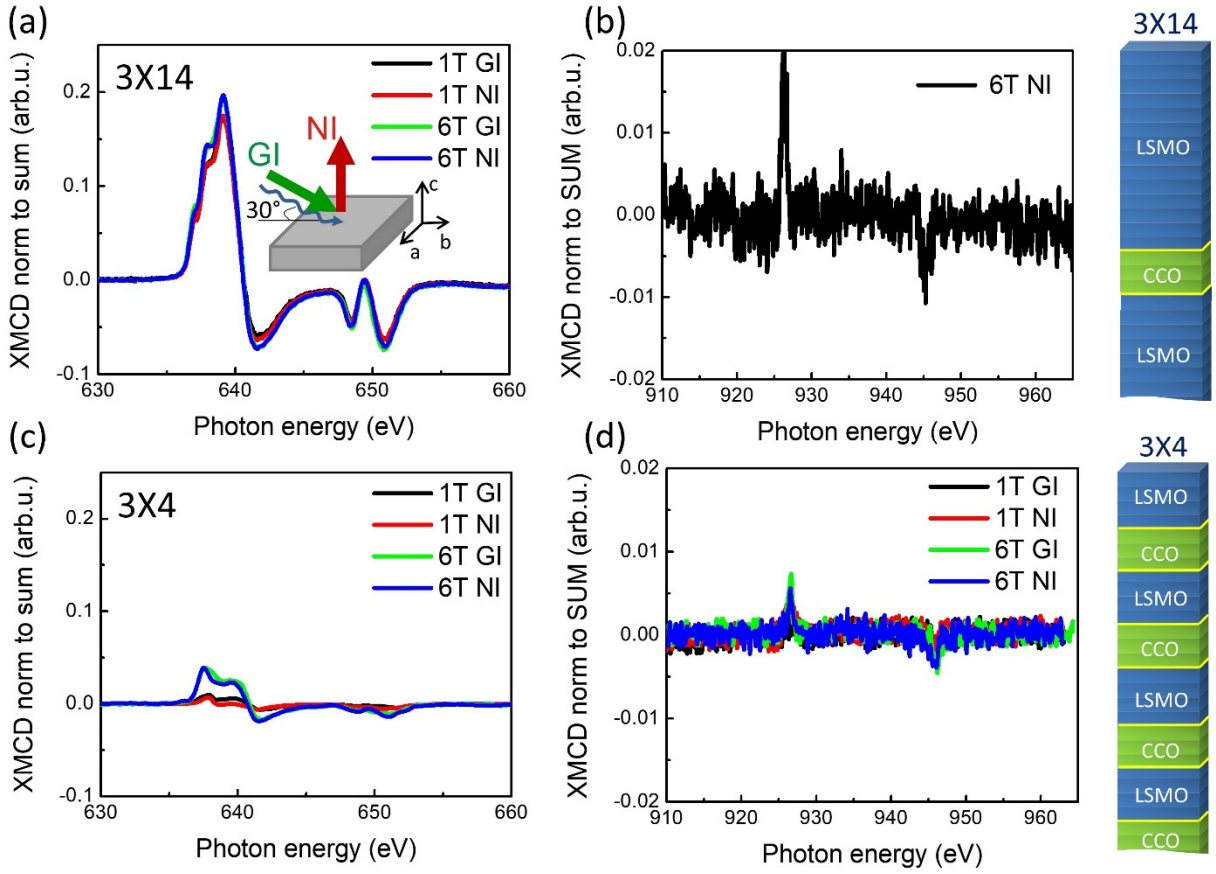

Figure 2. (a) and (b) Comparison between the XMCD at the Mn and Cu $L_{2,3}$-edges of 3×14 SL03. (c) and (d) Comparison between the XMCD at the Mn and Cu $L_{2,3}$-edges of 3×4 SL03. Temperature 30K, magnetic field 1 – 6 T. At each XAS edge the horizontal scale is the same for a better comparison of the spectra. Inset in panel (a) shows the direction of the magnetization and the applied magnetic field vectors in the grazing incidence (GI) and normal incidence (NI) configurations. Sketches of the number of probed layers in case of 3×14 and 3×4 SLs are drawn on the right. This roughly corresponds to the experimentally probed depth of about 10 nm.

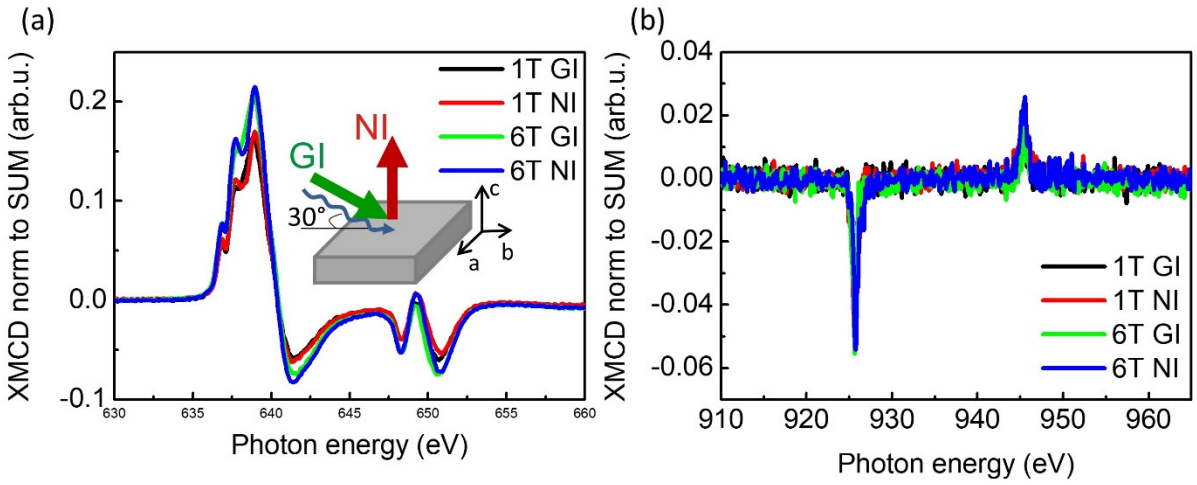

Figure 3. Comparison of the XMCD at the Mn (a) and Cu (b) $L_{2,3}$-edges of 3×14 SL01. Temperature 30K, magnetic field 1-6T.

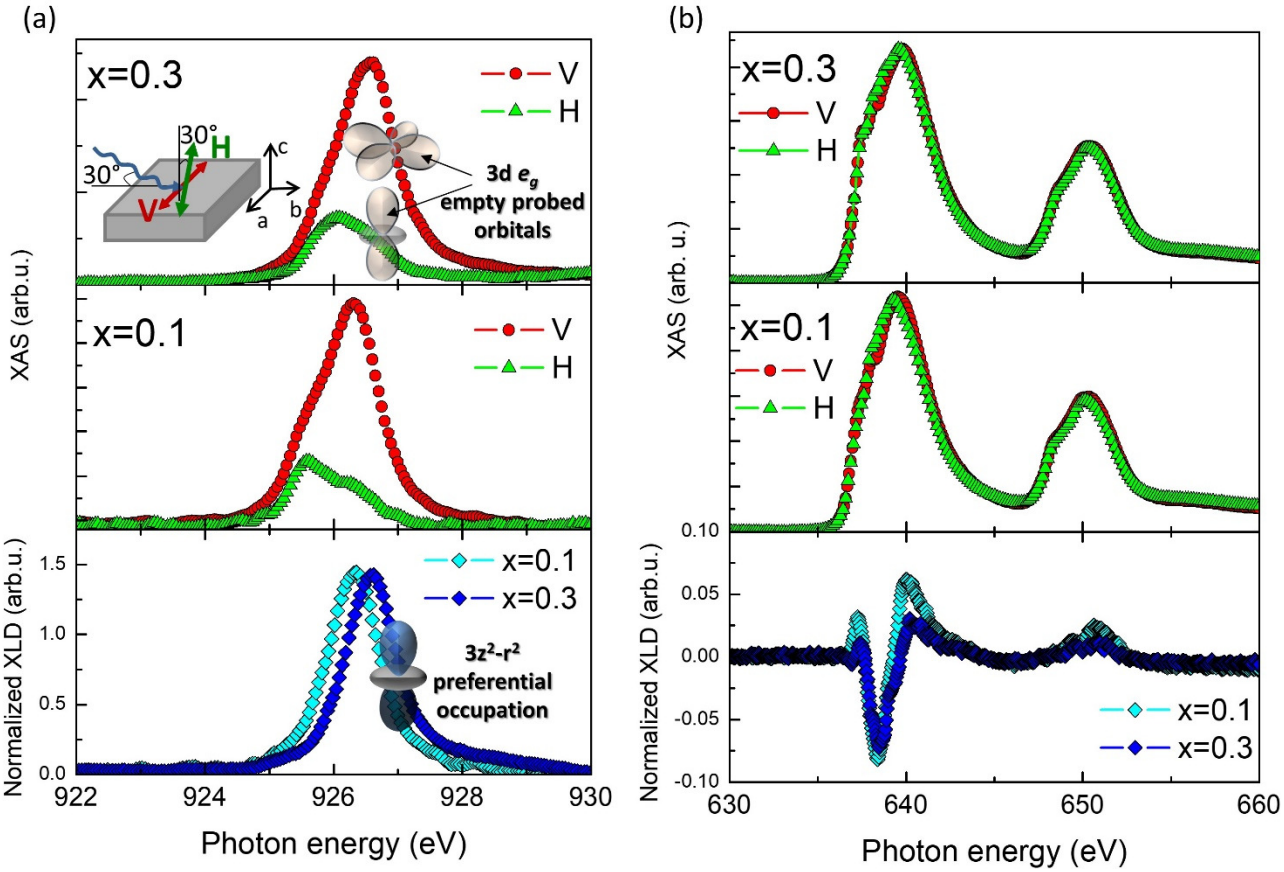

Figure 4. XAS at the Cu L_3 edge (panel a) and at the Mn $L_{2,3}$ edge (panel b) in GI with two orthogonal linear polarization V and H of 3×14 SL03 and 3×14 SL01 (top two panels) and XLD =V-H (bottom panel), measured at 300K temperature and without applied magnetic field.

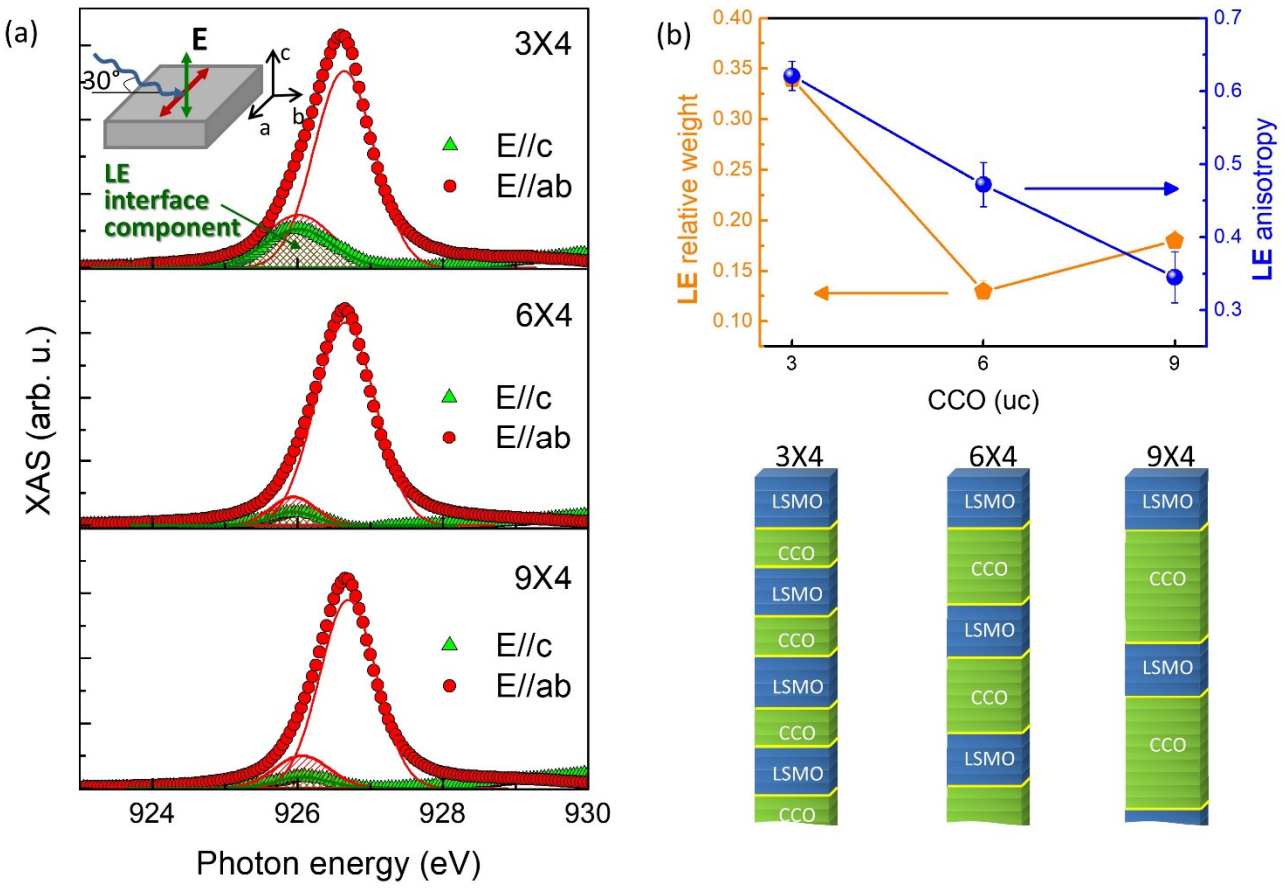

Figure 5. (a) XAS measurements and fit results at the Cu L_3 edge in GI of SL03s with fixed 4uc of LSMO and changing 3, 6, 9 uc of CCO: 3×4, 6×4 and 9×4. The curve with E//ab corresponds to the V polarization measurement, while the E//c component was isolated by combining the V and H polarization spectra. Temperature 300K, magnetic field 0 T. (b) Relative weight and anisotropy of the low energy component (LE) with different CCO thickness expressed in uc. The LE relative weight is defined as (Area($LE_{//ab}$)+Area($LE_{//c}$))/(total Area) and the LE anisotropy is defined as Area($LE_{//c}$)/Area($LE_{//ab}$).

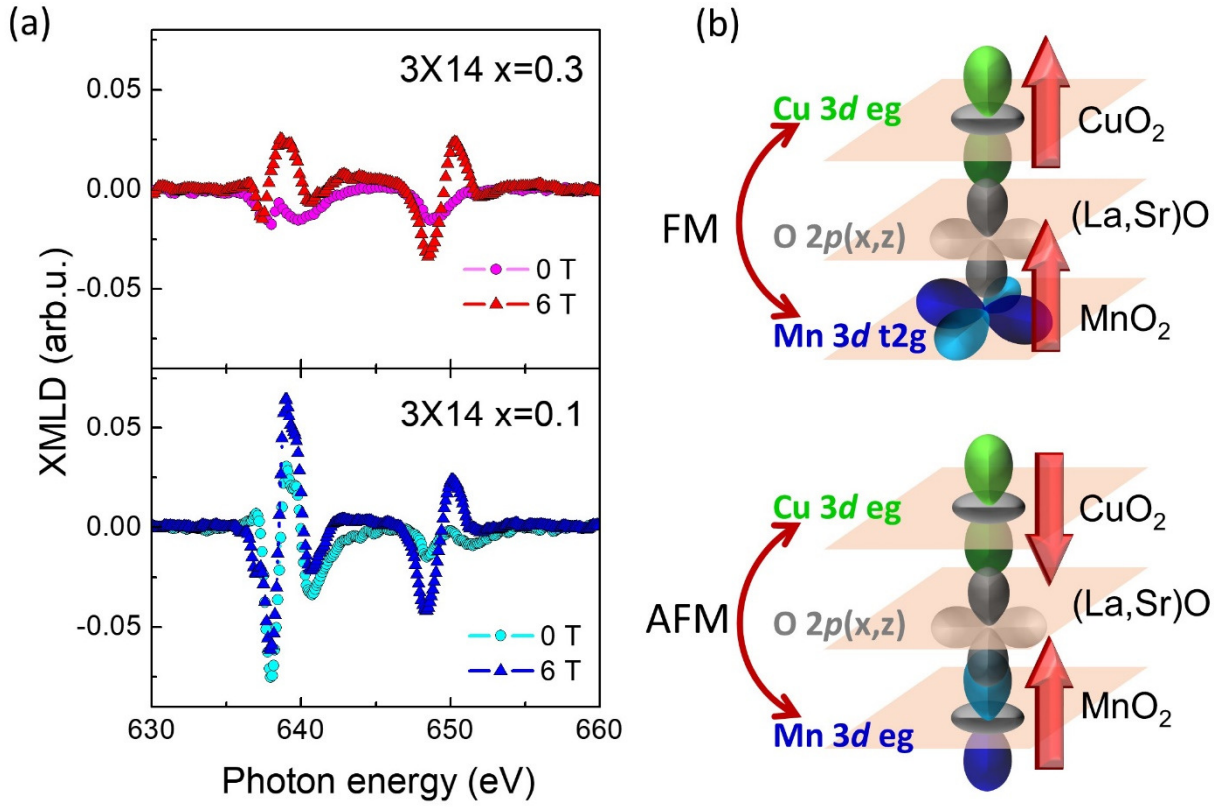

Figure 6. (a) XMLD at the Mn $L_{2,3}$ edge results for 3X14 SL03 and 3X14 SL01 with 6T and without (0 T) magnetic field. XMLD is obtained as the difference between the XLD at 30K and XLD at 300K. (b) Schematic representation of the preferentially occupied orbitals and the interfacial magnetic coupling close to the interface between the CCO and LSMO.

Table of contents entry

The cuprate/manganite interface shows different magnetic coupling depending on the manganite doping. The magnetic coupling is ferromagnetic or antiferromagnetic when the manganite is optimally doped or underdoped, respectively. The higher overlap of Cu 3*d* and Mn 3*d* bands driven by the larger Mn^{3+} content in the underdoped manganite facilitates the antiferromagnetic coupling between Cu 3*d*($3z^2$-r^2) and Mn 3*d*($3z^2$-r^2) orbitals.

Keyword interface magnetic interactions

Christoph Schlueter, Nan Yang, Claudio Mazzoli, Claudia Cantoni, Antonello Tebano, Daniele Di Castro, Giuseppe Balestrino, Pasquale Orgiani, Alice Galdi, Javier Herrero-Martín, Pierluigi Gargiani, Manuel Valvidares, and Carmela Aruta*

Orbital hybridization and magnetic coupling at cuprate-manganite interfaces driven by manganite doping

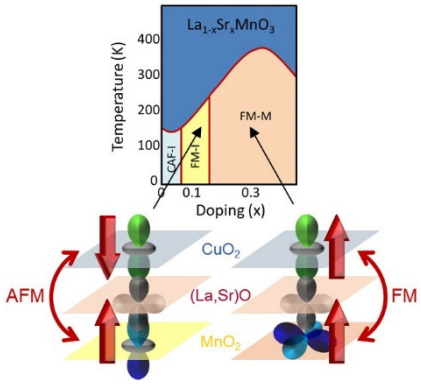

Supporting Information

Orbital hybridization and magnetic coupling at cuprate-manganite interfaces driven by manganite doping

*Christoph Schlueter, Nan Yang, Claudio Mazzoli, Claudia Cantoni, Antonello Tebano, Daniele Di Castro, Giuseppe Balestrino, Pasquale Orgiani, Alice Galdi, Javier Herrero-Martín, Pierluigi Gargiani, Manuel Valvidares, and Carmela Aruta**[*]

[1] Photon Science, Deutsches Elektronen-Synchrotron DESY, Hamburg, 22603, Germany
[2] School of Physical Science and Technology, ShanghaiTech University, 201210 Shanghai, China
[3] National Synchrotron Light Source III, Brookhaven National Laboratory, New York 11973, USA
[4] Materials Science and Technology Division, Oak Ridge National Laboratory, Oak Ridge, 37831 TN, USA
[5] Department DICII, University of Roma Tor Vergata, I-00133 Rome, Italy
[6] CNR-SPIN c/o University of Roma Tor Vergata, I-00133 Rome, Italy
[7] CNR-SPIN Salerno, University of Salerno, I-84084 Fisciano, Italy
[8] CNR-IOM, TASC National Laboratory, I-34149 Trieste, Italy
[9] CLASSE, Cornell University, Ithaca NY 14853, USA
[10] ALBA Synchrotron Light Source, Cerdanyola del Vallès, 08290 Barcelona, Spain

* Corresponding Author E-mail: carmela.aruta@spin.cnr.it

S1. X-ray diffraction

X-ray diffraction (XRD) measurements were routinely performed with a Rigaku D-max diffractometer and with a Philips X' Pert-XRD analytic diffractometer for higher intensity characterizations, using in both cases a Cu Kα source. The measurements were performed in symmetrical configuration after the alignment of the substrate crystallographic planes.

Since bulk manganites with both compositions x=0.3 and x=0.1 have the same pesudocubic value of 3.87 Å, [1] when the manganites are grown in the $CaCuO_2/La_{1-x}Sr_xMnO_3$ (CCO/LSMO) superlattices (SLs) on the well matched (110)$NdGaO_3$ (NGO) substrate (pseudocubic in-plane lattice parameter *a* = 3.87 Å), no significant differences can be detected by XRD between the x=0.3 and the x=0.1 cases. XRD spectra of the 3×4, 6×4 and 9×4 CCO/LSMO SLs with x = 0.3 are reported in Figure S1 in the angular range around the (002) Bragg reflection of NGO substrate. The periodicity of the superstructure can be calculated by the formula

$$\Lambda = n_1 \cdot c_{CCO} + n_2 \cdot c_{LSMO}$$

where n_1 (n_2) and c_{CCO} (c_{LSMO}) are the unit cells (uc) and the c-axis parameter of CCO (LSMO), respectively. The average lattice parameter can be obtained by the Bragg law applied to the SL_0 peak. The red thicks indicate the calculated angular positions of the satellite peaks $SL_{\pm i}$ and the average

structure peak SL_0.[2, 3] The satellite peaks $SL_{\pm i}$ up to high order are clearly visible indicating the good structural quality of the SLs.

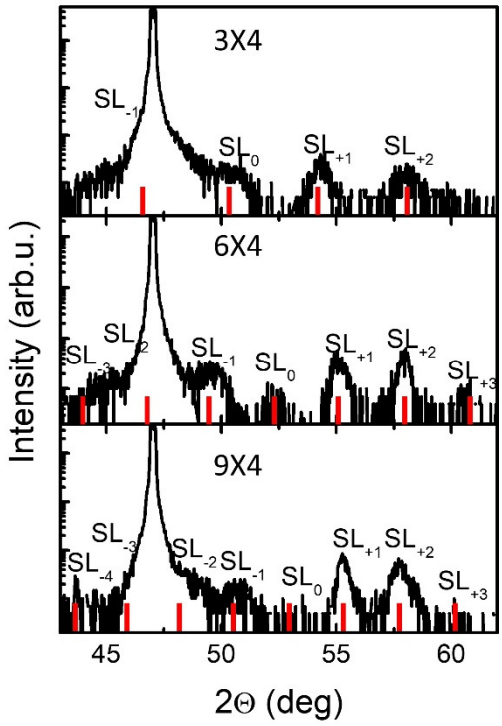

Figure S1. XRD Θ/2Θ scans in logarithmic scale of the 3×4, 6×4 and 9×4 CCO/LSMO SLs with x = 0.3 around the NGO substrate (002) Bragg reflection by a Rigaku D-max diffractometer using Cu Kα radiation. The red ticks indicate the calculated positions of the satellite peaks $SL_{\pm i}$ and the average structure peak SL_0.

XRD spectra for 3×14 and 3×4 CCO/LSMO SLs with x = 0.3 (3×14 SL03 and 3×4 SL03) measured with higher x-ray intensity are reported in Figure S2 (a) together with the low angle x-ray reflectivity (XRR) measurements in Figure S2 (b). In the graphs the simulation (red curves) are also reported. They were obtained with the *InteractiveXRDFit* program for XRD data [4] and the IMD package of XOP software for XRR data.[5, 6] XRD and XRR measurements confirm the 3×14 and 3×4 periodicity with c_{CCO} about 3.25 Å and c_{LSMO} about 3.87 Å. In the case of the XRR simulation an interface roughness of 1uc was considered. Due to resolution limitation of our diffractometer a careful analysis of the interface roughness cannot be provided. XRR oscillations are visible up to 2θ value of about 4°, above it, fall below the experimental resolution of the X-ray diffractometer. However, the XRR oscillations eventually merge into size-effect oscillations around the I and II order SLs Bragg reflections.

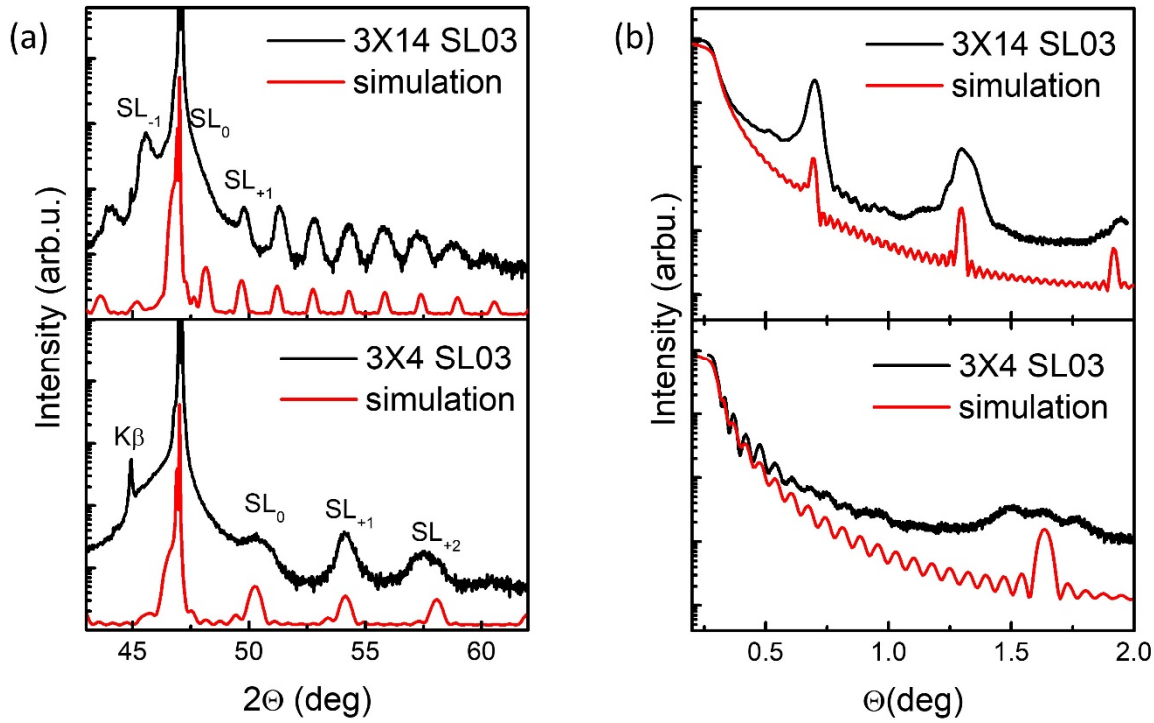

Figure S2. (a) XRD Θ/2Θ scans of the 3×14 SL03 and 3×4 SL03 around the (002) Bragg reflection of NGO substrate. (b) XRR measurements on the same samples. Both measurements were performed by Philips X'Pert-XRD analytic diffractometer using a Cu Kα source. XRD and XRR curves obtained by simulations are also included (red lines).

S2. Fit of X-ray absorption at Cu L_3 edge in 3×14 SLs with different doping

X-ray absorption (XAS) spectra at Cu L_3 edge (Cu $2p \rightarrow$ Cu $3d$ electron transition energy) for 3×14 SL03 and 3×14 SL01 are reported in Figure S3.

The V and H polarization spectra were combined to isolate the E//c component. The E//ab data were fitted with two Gaussian curves, corresponding to the bulk and interface Cu^{2+} components, while the E//c spectrum only contains the interface contribution. The energy position and width of the interface component were fixed to the values obtained by the fit of the single Gaussian peak in the E//c data, and only allowing its intensity to vary.

The relative weight of the interface component at lower energy, defined as (Area($LE_{//ab}$)+Area($LE_{//c}$))/(total Area), results to be ≅0.39 and 0.37 for 3×14 SL03 and 3×14 SL01, respectively.

The anisotropy of the same component, defined as Area($LE_{//c}$)/Area($LE_{//ab}$), results ≅0.8 and 0.34 for 3×14 SL03 and 3×14 SL01, respectively.

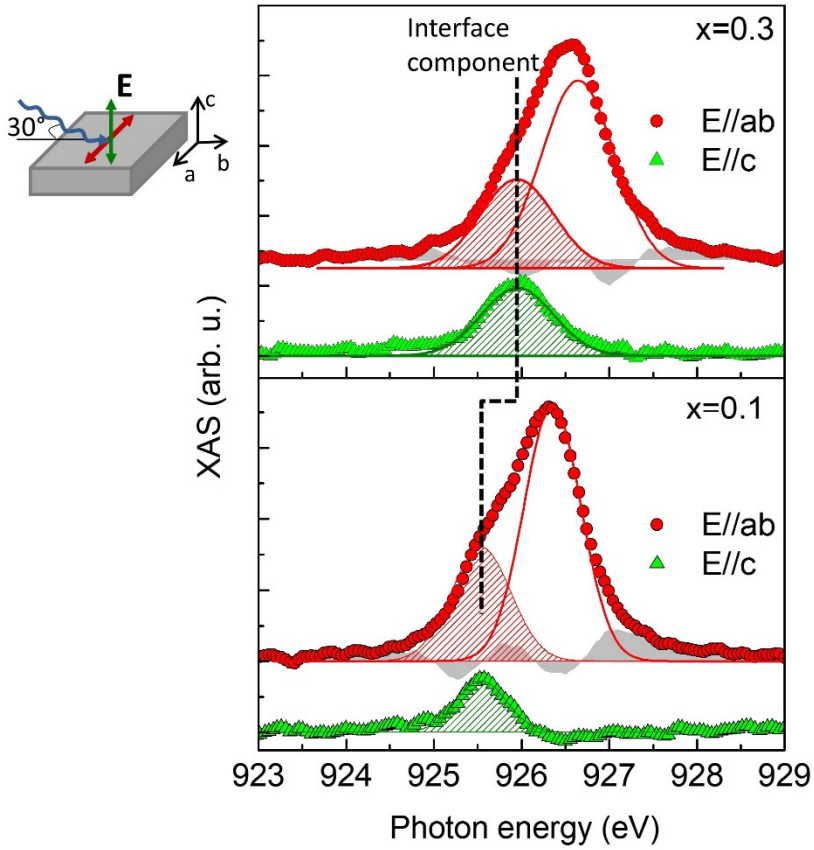

Figure S3. XAS at the Cu L_3 edge in GI with two orthogonal linear polarization V and H of 3×14 SL03 and 3×14 SL01, measured at 300K temperature and without applied magnetic field. Spectra are fitted with two components for E//ab and one component for E//c (interface component). The dashed grey areas correspond to the residuals of the fits.

S3. XAS at Mn $L_{2,3}$ edge in SLs with different LSMO thickness and doping

Isotropic XAS spectra at the Mn $L_{2,3}$ edges (Mn $2p\rightarrow$ Mn $3d$ electron transition energy) of SLs with different LSMO thickness and doping are reported in Figure S4. The isotropic spectra are obtained as $(V-H)/2$ and normalized to unity, to better highlight the shift at higher photon energy of the 3×4 SL03 with respect to 3×14 SL03 because of the enhancement of Mn^{4+} content at the interface. However, the spectrum of 3×14 SL01 shifts to lower photon energy with respect to 3×14 SL03 because of the enhancement of Mn^{3+} in the underdoped manganite. The XLD spectra are also shown, which are obtained as the difference between the two XAS measurements $(V-H)$, after linear background subtraction at the pre-edge region of the L_3 edge and normalization to the edge jump set to unity above the L_2 edge.

The shape of XLD spectra gives information on the symmetry of the preferentially occupied 3d e_g orbitals. All measured SLs showed similar XLD shapes, which are typical of the preferential occupation of the out-of-plane $3z^2$-r^2 orbitals. The comparison between SLs with different LSMO thickness also shows that the thinner LSMO the more dichroic it is. This indicates that the $3z^2$-r^2

orbital preferential occupation is mainly an interface effect. However, the increased Mn^{3+} content in the case of underdoped manganite gives rise to an even higher $3z^2$-r^2 orbital preferential occupation.

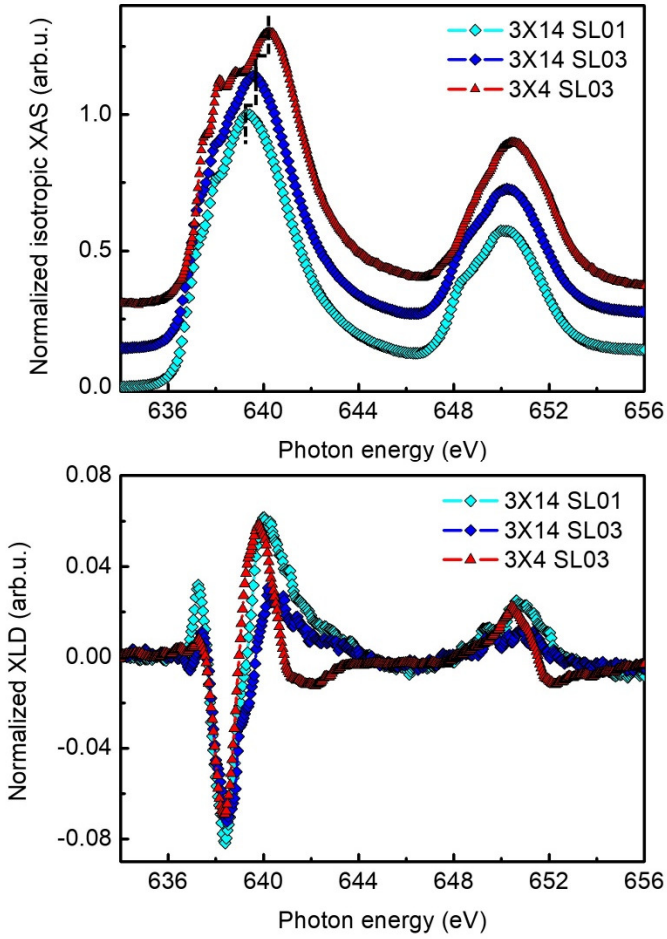

Figure S4. (Top panel) Normalized to unity isotropic XAS measurements at the Mn $L_{2,3}$ edge of 3×14 SL01, 3×14 SL03 and 3×4 SL03. The spectra are shifted for clarity. (Bottom panel) XLD spectra obtained from the XAS measurements as in the top. Measurements are performed at 300K temperature and without applied magnetic field.

References

[1] A. Urushibara, Y. Moritomo, T. Arima, A.Asamitsu, G. Kido, Y. Tokura, *Phys. Rev. B* **1995**, *51*, 14103.

[2] D. Di Castro, M. Salvato, A. Tebano, D. Innocenti, C. Aruta, W. Prellier, O. I. Lebedev, I. Ottaviani, N. B. Brookes, M. Minola, M. M. Sala, C. Mazzoli, P. G. Medaglia, G. Ghiringhelli, L. Braicovich, M. Cirillo, and G. Balestrino, *Phys. Rev. B* **2012**, *86*, 134524.

[3] N. Yang, D. Di Castro, C. Aruta, C. Mazzoli, M. Minola, N. B. Brookes, M. Moretti Sala, W. Prellier, O. I. Lebedev, A. Tebano,1 and G. Balestrino, *J. of Appl. Phys.* **2012**, *112*, 123901.

[4] Céline Lichtensteiger, *J. Appl. Cryst.* **2018**, *51*, 1745–1751.

[5] D.L. Windt, *Comput. Phys*. **1998**, *12*, 360.

[6] M. Sanchez del Rio, R.J. Dejus, *SPIE Proc.* **2011**, *8141*, 814115.